



Trinity College Dublin  
Coláiste na Tríonóide, Baile Átha Cliath  
The University of Dublin

# Design Study of a Compact Quadrupole Doublet for a kHz Repetition Rate Laser-Plasma-Accelerator

Aaditya Vedant, Trinity College Dublin, Ireland

MLS Group

September 7, 2022

## Abstract

The MLS group at DESY is building the KALDERA laser, a kHz repetition rate, high power laser system for the purpose of laser-wakefield acceleration. In a first experimental phase with reduced output power, first studies towards active stabilization of the driver laser and the electron beam properties will be performed. A compact quadrupole doublet is required to capture the electron beams as early as possible and to therefore preserve the beam quality during transport to subsequent experiments. In this report the basic layout of this doublet is optimized towards maximum focusable electron energy, while ensuring a clip free transmission of the remaining kHz laser. The magnets should be placed as close to the plasma source as 10 cm and 15 cm apart, in order to be able to focus beam energies as high as 240 MeV.

# Contents

<b>1</b>	<b>Introduction</b>	<b>3</b>
<b>2</b>	<b>Theory</b>	<b>4</b>
2.1	Laser Driven Plasma Wakefield Acceleration . . . . .	4
2.2	Charged Beam Focusing . . . . .	5
2.2.1	Quadrupole Magnets . . . . .	5
2.2.2	Trajectory of an electron in the beamline . . . . .	8
2.2.3	Beam size focusing . . . . .	9
<b>3</b>	<b>Experimental Setup</b>	<b>10</b>
3.1	Magnet Schematic . . . . .	10
3.2	Magnet Gradients . . . . .	11
<b>4</b>	<b>Results</b>	<b>12</b>
4.1	Beam Tracking . . . . .	12
4.2	Energy Focusing . . . . .	14
<b>5</b>	<b>Conclusion</b>	<b>16</b>
<b>6</b>	<b>Acknowledgements</b>	<b>17</b>

# 1 Introduction

Modern particle accelerators are drivers for state-of-the-art research applications in physics, industry, medicine, and other branches of society.

Conventional accelerator technology is based on utilizing the electric field of radio frequency waves inside a resonator cavity so as to accelerate particle beams to highly relativistic energies.

Aiming for highest particle energies, the maximum achievable electric field, of the order of 100 GeV/m, results in accelerator lengths of the orders of several kilometers.

Naturally, the costs for these large scale facilities grow on a similar scale, which results in them being built less frequently than these important tools are needed to be built.

A promising alternative technology to accelerate electrons is the so called laser-plasma acceleration [1, 2]. Here, a high intensity laser pulse is used to create a plasma density modulation, i.e. a plasma wakefield. The arising electric fields of order of 100 GeV/m can be used to accelerate electrons in the direction of the laser and thus drastically reduce the footprint of the accelerator and therefore its costs.

However, plasma accelerators are still in development. High energy [3], high charge [4], low emittance [5], and temporally short beams [6] out of the plasma have already been demonstrated. But open challenges remain, i.e. large beam divergences of the order of 1 mrad, 1 %-level energy spreads and shot-to-shot instabilities in beam quality.

The MLS group at DESY is operating a laser-plasma accelerator called LUX and aims to improve this new technology towards stability and beam quality [7]. The LUX accelerator is driven by the 100 TW class ANGUS laser system and features a novel plasma-source attached to a conventional accelerator beamline, including a short period undulator. The ultimate goal is to demonstrate free-electron lasing from plasma accelerated beams, which would benchmark the high quality and stability of the generated electron beams.

The stability of the electron beams is highly dependent on the shot-to-shot stability of the driving laser pulses [8]. State-of-the-art high intensity laser systems are typically limited to a 1-10 Hz repetition rate. In order to push the limits in terms of laser and electron beam stability, the MLS group is developing a new up to 1 kHz repetition rate laser system, called KALDERA, which will, for the first time, allow for active stabilization of the electron quality by mitigating disturbances by vibrations and air turbulence in the laser system.

In the first experimental phase of KALDERA, that will deliver full repetition rate but reduced laser power, first plasma-acceleration experiments will be performed at the PIP accelerator. Though highest electron beam quality can not be expected from the intermediate state laser driver, first studies towards active stabilization can be utilized. In order to account for the reduced laser intensity on target, a short focal length of the final focusing mirror is required. Further, comparably low electron energies between 50

MeV and 200 MeV are expected, causing a comparably large relative energy spread of 2-4 % and comparably large electron divergences of 2-4 mrad.

The combination of high energy spread and beam divergence make the transport of the electron beam a challenge. In particular, the beam emittance degrades during free drift space in the presence of both the high energy spread and divergence [9]. Therefore, to reduce the beam divergence, it is highly important to focus the beams after the plasma source as early as possible.

The aim of this report is the designing of a focusing quadrupole doublet behind the plasma source to fulfill this requirement. On one hand, the required field strength of the quadrupole magnets to focus the electron beam increases the closer the magnets are placed to the plasma source. On the other hand, the high intensity, kHz repetition rate laser pulses diverging from the plasma need to pass the magnet apertures clip free, in order to avoid damage and to allow for a subsequent detection of the laser pulses after the plasma interaction. However increasing the aperture of the quadrupole magnets lowers the achievable field strength. The challenge was to maximize the total beam energy that still can be focused while keeping the clear aperture at the respective magnet positions.

A brief introduction into the principle physics of laser plasma acceleration is given in section 2.1. The basic properties of quadrupole magnet lenses are described in section 2.2.1 followed by a short introduction into particle beam transport in section 2.2.2.

The planned experimental setup and the parameters of interest for this study are presented in section 3. The main results of the design study are finally shown in section 4 which is followed by a short conclusion.

## 2 Theory

### 2.1 Laser Driven Plasma Wakefield Acceleration

This method involves sending a short laser pulse in a plasma medium to drive the electrons and accelerate them. When a laser beam enters the Plasma medium, the photon momentum creates radiation pressure and as the laser propagates through, the pressure displaces the electrons within the plasma. The ions remain unchanged due to their higher mass. This is analogous to a speedboat travelling through a pond, displacing the water ahead of it and pushing it to the sides. The speedboat is the laser beam, and the water is the plasma in this analogy (Figure 1).

A wake is described as the wave that is created behind the moving body as it propagates through the medium. Figure 2 best demonstrates it in the context of the boat analogy provided here.

The laser propagating through the plasma displaces the electrons out of its path, as a result of the pondermotive force created by the oscillating electromagnetic field of the laser. Due to the pondermotive force, a wake is created behind the travelling photons.

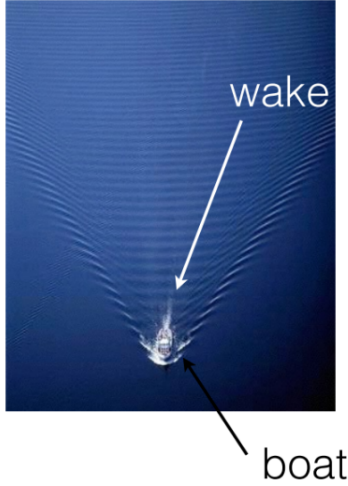


Figure 1: A boat driving through the water, creating wakes behind it [10]

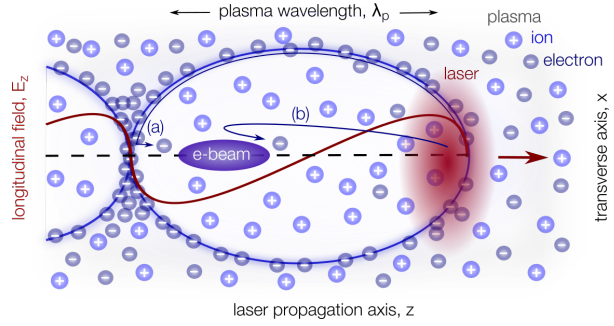


Figure 2: Creation of wakes in a plasma as the laser drives through it (Courtesy of P. Winkler)

Within the wake, the separation of charges creates large longitudinal electric fields that scale with the electron density  $n_0$  as [2]:

$$E_z [GV/m] \simeq 96 \cdot \sqrt{n_0 [10^{18} cm^{-3}]}$$

For typical electron densities of  $10^{18} cm^{-3}$  the electric field is on the order of 100 GV/m, and can be used to accelerate an injected electron beam in the direction of the laser.

The laser drives and accelerates the electron beam until a given point, where it then exits the plasma and the electron beam is propagated and diverted towards the experiment.

## 2.2 Charged Beam Focusing

### 2.2.1 Quadrupole Magnets

As mentioned in the introduction, reduction of the beam divergence is crucial to maintain the beam quality during transport.

The magnets used for beam focusing come in various types, which can be classified on the number of poles they have. It is not unusual to use a dipole magnet for beam bending and deflection purposes, while Quadrupoles are used for beam focusing. This report focuses on the use of quadrupole magnets to focus the beam and therefore reduce the electron beam divergence.

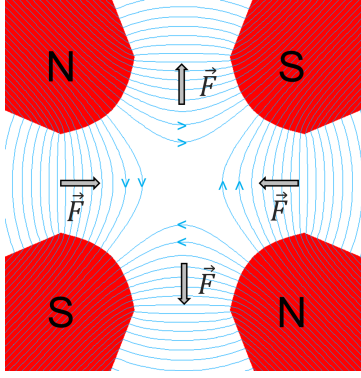


Figure 3:  
Schematic of magnetic field within a  
quadrupole magnet  
(Courtesy of P. Winkler)



Figure 4:  
Quadrupole magnet used in the LUX  
beamline  
(Courtesy of P. Winkler)

Shown in figure 3, the quadrupole magnet has four poles, where the same poles are opposite each other. This configuration results in a net magnetic field such that the strength is proportional to the distance from the centre of the magnet [11]. The fields can be described by:

$$B_y = -g x \quad B_x = g y$$

The gradient of the quadrupole magnet is the slope of the magnetic field along the transverse distance from the centre (origin). Since the field strengths are proportional to the distance from the centre, there is no magnetic field at the centre of the magnet. In contrast to an optical lens, the quadrupole magnet focuses in one dimension but defocuses the beam in the other dimension by the same amount.

The gradient of the quadrupole magnet is related to the current flowing through it by:

$$g = \frac{2\mu_0 n I}{r^2} \quad (1)$$

Where  $\mu_0$  is the vacuum permeability,  $n$  is the number of turns of wire in the coil,  $I$  is the current flowing through it, and  $r$  is the aperture radius of the quadrupole. The equation indicates that the gradient scales linearly with the current, however that is only true up to a certain current, after which saturation effects set in and the gradient scales nonlinearly with the current. The gradient scaling at high currents is determined experimentally.

The gradient of a magnet can also be related to its strength. For a quadrupole, it is given by

$$k = \frac{eg}{p}$$

Where  $k$  is the magnet strength,  $e$  is the charge of an electron,  $g$  is the magnet gradient, and  $p$  is the electron momentum. The strength of a magnet can also be related to the electron energy via the momentum energy relation.

$$E^2 = m^2 c^4 + p^2 c^2$$

The energy of a particle is on the order of  $GeV$ . The first thing is to divide both sides of the equation by the speed of light squared  $c^2$ .

$$\frac{E^2}{c^2} = m^2 c^2 + p^2$$

Thus the Energy of an electron can be expressed as:

$$\frac{E}{c} = \sqrt{m^2 c^2 + p^2}$$

It is known that the mass of an electron (hence the rest energy) is extremely small compared to its momentum, thus  $m^2 c^2 = m(m c^2) \ll p^2$ . Therefore, the Energy equation is:

$$\frac{E}{c} \approx \sqrt{p^2} \approx p$$

Hence, for an electron, the Energy divided by speed of light is approximately equal to the particle momentum. Thus, inputting units, it can be stated that

$$E[GeV] = p[GeV/c]$$

This can now be substituted into the magnet strength.

$$k[m^2] \propto \frac{g[T/m]}{E[GeV]}$$

To account for the addition of the  $c$  term, a proportionality factor is added to the equation.

$$k[m^2] = 0.2998 \frac{g[T/m]}{E[GeV]} \quad (2)$$

Hence, the magnet strength is inversely proportional to the energy of the electrons it can focus.[12]

For the reason of the quadrupole focusing in one plane only, often two or more quadrupoles are used in conjunction with each other. A quadrupole doublet is a popular choice. Two quadrupoles, one focusing, and the other defocusing are used in series with each other. The overall effect is that of focusing the beam in both dimensions. The first one focuses in the  $x$  plane and the second in the  $y$  plane. Even in a single dimension, the structure has an overall focusing effect. This effect can be observed in Figure 7.

### 2.2.2 Trajectory of an electron in the beamline

The trajectory of a particle within a beamline containing both quadrupoles and drift spaces (free space) can be described entirely by transport matrices [13]. Suppose a particle in the beamline with initial position  $x_0$  and angle relative to the ideal trajectory  $x'_0$ . The drift transport matrix is:

$$M_d = \begin{bmatrix} 1 & s \\ 0 & 1 \end{bmatrix}$$

Where  $s$  is the length drifted by the particle in free space. The updated set of coordinates of the particle as drifting in free space for a length  $s$  are given by:

$$\begin{bmatrix} x \\ x' \end{bmatrix} = \begin{bmatrix} 1 & s \\ 0 & 1 \end{bmatrix} \begin{bmatrix} x_0 \\ x'_0 \end{bmatrix}$$

Now, if the particle were to traverse through a quadrupole, the trajectory would be affected by the magnetic field. The coordinates of the particle after it has been through a focusing ( $K > 0$ ) magnet are given by the matrix transformation:

$$\begin{bmatrix} x \\ x' \end{bmatrix} = \begin{bmatrix} \cos(l\sqrt{|K|}) & \frac{1}{\sqrt{|K|}}\sin(l\sqrt{|K|}) \\ -\sqrt{|K|}\sin(l\sqrt{|K|}) & \cos(l\sqrt{|K|}) \end{bmatrix} \begin{bmatrix} x_0 \\ x'_0 \end{bmatrix}$$

where  $l$  is length of the magnet and  $K$  is the magnet strength. For a defocusing magnet ( $K < 0$ ):

$$\begin{bmatrix} x \\ x' \end{bmatrix} = \begin{bmatrix} \cosh(l\sqrt{|K|}) & \frac{1}{\sqrt{|K|}}\sinh(l\sqrt{|K|}) \\ \sqrt{|K|}\sinh(l\sqrt{|K|}) & \cosh(l\sqrt{|K|}) \end{bmatrix} \begin{bmatrix} x_0 \\ x'_0 \end{bmatrix}$$

The same matrix transformations are used for the trajectory of the particle in the  $y$  direction with initial coordinates

$$\begin{bmatrix} y_0 \\ y'_0 \end{bmatrix}$$

However, it is important to note that as mentioned before, if a quadrupole focuses the particle in the  $x$  direction, it will defocus it in the  $y$  direction. Hence a  $4 \times 4$  matrix can be constructed for a magnet, and drift space.

For  $K > 0$ :

$$M_F = \begin{bmatrix} \cos(l\sqrt{|K|}) & \frac{1}{\sqrt{|K|}}\sin(l\sqrt{|K|}) & 0 & 0 \\ -\sqrt{|K|}\sin(l\sqrt{|K|}) & \cos(l\sqrt{|K|}) & 0 & 0 \\ 0 & 0 & \cosh(l\sqrt{|K|}) & \frac{1}{\sqrt{|K|}}\sinh(l\sqrt{|K|}) \\ 0 & 0 & \sqrt{|K|}\sinh(l\sqrt{|K|}) & \cosh(l\sqrt{|K|}) \end{bmatrix}$$

For  $K < 0$ :

$$M_{DF} = \begin{bmatrix} \cosh(l\sqrt{|K|}) & \frac{1}{\sqrt{|K|}}\sinh(l\sqrt{|K|}) & 0 & 0 \\ \sqrt{|K|}\sinh(l\sqrt{|K|}) & \cosh(l\sqrt{|K|}) & 0 & 0 \\ 0 & 0 & \cos(l\sqrt{|K|}) & \frac{1}{\sqrt{|K|}}\sin(l\sqrt{|K|}) \\ 0 & 0 & -\sqrt{|K|}\sin(l\sqrt{|K|}) & \cos(l\sqrt{|K|}) \end{bmatrix}$$

For  $K = 0$  (drift):

$$M_D = \begin{bmatrix} 1 & s & 0 & 0 \\ 0 & 1 & 0 & 0 \\ 0 & 0 & 1 & s \\ 0 & 0 & 0 & 1 \end{bmatrix}$$

The advantage of using matrix transformations to describe the trajectory of the particle through each element of the beamline is that one single matrix transformation can be performed to produce the coordinates of the particle at any point in the beamline.

The transformation matrices can represent an arbitrary sequence of drift spaces and quadrupoles. Let  $\mathcal{M}_i$  represent a transport matrix for an element (drift space or quadrupole).

Supposing the above sequence of beamline elements, one can construct a final transport matrix  $\mathcal{M}_{tot}$  that gives the coordinates of the particle at the end of the sequence.

$$\mathcal{M}_{tot} = \mathcal{M}_n \dots \mathcal{M}_4 \mathcal{M}_3 \mathcal{M}_2 \mathcal{M}_1$$

The final coordinates will be

$$\begin{bmatrix} x \\ x' \end{bmatrix} = \mathcal{M}_{tot} \begin{bmatrix} x_0 \\ x'_0 \end{bmatrix}$$

Hence, as the sequence of elements are known, using the transport matrices, the trajectory at any point in the beamline can be calculated. [14]

### 2.2.3 Beam size focusing

An electron beam contains a large number of particles, each with different set of coordinates. It is thus difficult and impractical to calculate the trajectories of individual particles, as we are interested in the beam as a whole [15].

Liouville's theorem states that the area of the beam in the phase space (emittance) is conserved. This allows us to determine the area and distribution of the beam at any point in the beamline, given that we know the emittance [15]. Mathematically,

$$u^T \Sigma^{-1} u = 1$$

where

$$u = \begin{bmatrix} x \\ x' \\ y \\ y' \end{bmatrix}$$

and

$$\Sigma = \begin{bmatrix} \langle x_i^2 \rangle & \langle x_i x_i' \rangle \\ \langle x_i' x_i \rangle & \langle x_i'^2 \rangle \end{bmatrix}$$

$\langle x_i^2 \rangle$  is square of the beam size and  $\langle x_i'^2 \rangle$  is the square of the beam divergence. We assume the particles position and angle out of the plasma having no correlation  $\langle x_i' x_i \rangle = 0$ . Hence the  $\Sigma$  covariance matrix carries the beam parameters.

In the exact fashion as before, the transformation matrix for all the beamline elements  $\mathcal{M}_{tot}$  can operate on the covariance matrix to update the beam parameters at all points in the beamline.

$$\Sigma = \mathcal{M}_{tot} \Sigma_0 \mathcal{M}_{tot}^T$$

## 3 Experimental Setup

### 3.1 Magnet Schematic

This section covers the numbers associated with the parameters of the laser and the electron beam such as initial beam size and divergence, laser divergence, and the distances between beamline elements.

Figure 5 demonstrates the laser beam, with the electron beam enveloped inside it, traversing through the quadruple doublet. A mirror then deflects the laser out of the beamline while the electron beam continues towards the target.

Table 1 summarizes the important experimental parameters.

Table 1: Electron beam and Magnet Parameters

Parameters	Values
Initial Beam size in x	5 $\mu\text{m}$
Initial Beam size in y	5 $\mu\text{m}$
Initial Beam divergence in x	20 mrad
Initial Beam divergence in y	20 mrad
Quadrupole 1 yoke length	10 cm
Quadrupole 2 yoke length	10 cm
Distance between yoke centers of both Quadrupoles	10 cm
Distance of Quadrupole 1 from the origin	15 cm
Distance of Quadrupole 2 from the origin	35 cm

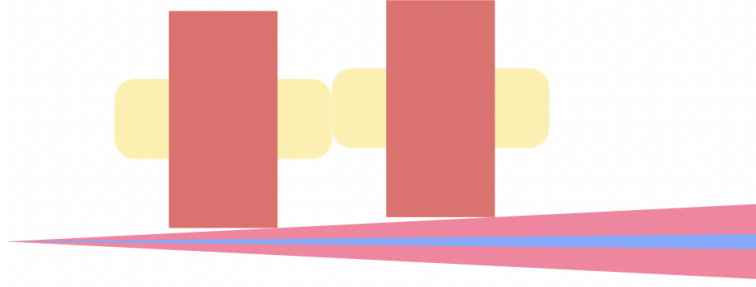


Figure 5: Schematic of laser and electron beam leaving the source through the beamline (Courtesy of M. Kirchen). Image shows the magnets yokes (red), coils (yellow), electron beam (blue), laser beam (pink)

It is important to note that the "Distance of Quadrupole from the origin" measures the distance between the origin (exit source) and the beginning of the yoke.

### 3.2 Magnet Gradients

It was seen in section 2.2.1 that the gradient of the magnet is mainly dependent on its aperture radius and the current that flows through it. This indicates that it is linearly proportional to the current. However, this is the case for only smaller currents. At larger currents, the magnetisation of the yoke begins to saturate, and the gradient no longer varies linearly with current.

From experimental data with one of the SQAs (Quadrupole), we extracted the gradient the magnets would have at a maximum possible current of  $I = 300$  A.

Figure 6 contains a scatter plot of the experimental data, with a gradient value for every 1 A. Over the scatter plot, is a interpolation curve of the data.

The radius of aperture of the magnet used to obtain the data was  $r = 20$  mm.

From the interpolation curve, it is obtained that at  $I = 300$  A, for this magnet,  $g = 33.5$  T/m. At this point however, one must specify the difference between the length of the magnet used in the experiment, and the effective length.

The above mathematics is based on the hard edge model of the magnet, i.e., the field of the magnet begins at the edge of the magnet, and abruptly ends at the other edge, like a step function. Realistically however, the field profile is much more continuous and begins before the edge of the magnet yoke.

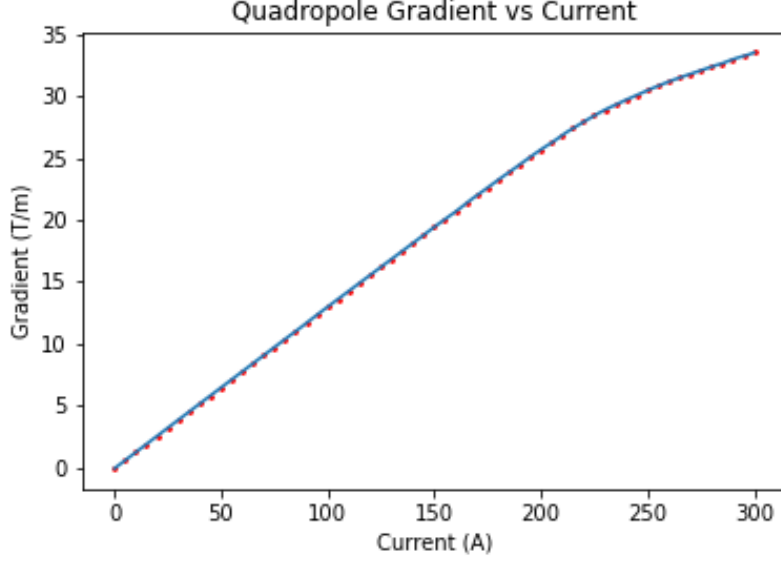


Figure 6: Variation of Quadrupole gradient with current (Courtesy of L.Hubner, MLS Group)

The gradient measured in figure 6 is the peak gradient. This means that what is measured is the peak gradient of the magnetic field profile. To adapt this to the hard edge model, we must multiply it with the ratio of the effective length  $l = 0.13473$  m to the yoke length of 0.100 m to make sure we get the integrated gradient of the field profile, hence approximating it to the what the gradient would be in the hard edge model.

Hence the gradient at  $I = 300$  A is  $33.5 * \frac{0.13473}{0.10000} = 45.2$  T/m

The gradient then has to be scaled with the desired aperture radius  $r_{new}$ . Hence using equation 1,

$$\frac{g_{scaled}}{g_0} = \frac{r_0}{r_{new}}$$

where  $g_0 = 45.2$  T/m, and  $r_0 = 20$  mm.

## 4 Results

### 4.1 Beam Tracking

This section will explore the trajectory of the beam as it passes through the magnets. The goal was to minimize the beam size at a distance of 2m from the origin. The simulation of the beam trajectory demonstrates the efficiency of the Quadrupole doublet at minimizing the beam size. The simulation is given an arbitrary value of the magnet positions (Table 1, except first drift distance), and it works on beam size

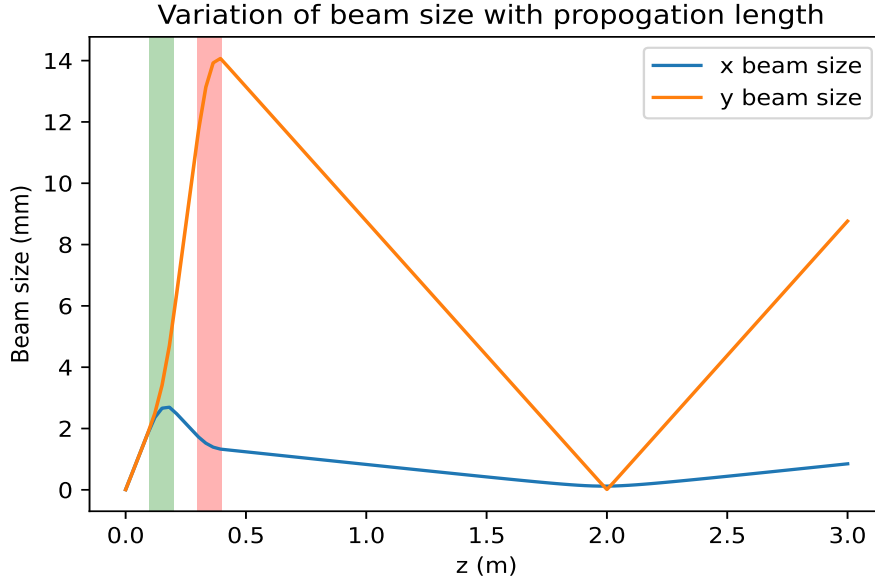


Figure 7:

Beam size variation through the beamline and the two Quadrupoles (Green, Red)

minimization by optimizing the strength  $K$  of the magnets. The first quadrupole (green) is focusing, while the second (red) is defocusing.

The beam starts off with the same size in both  $x$  and  $y$ , and the sizes increase in the same, linear fashion in the first drift space.

Once the beam reaches the first magnet, the contrasting focusing effects can be seen, as the beam size in the  $x$  direction reduces, but the  $y$  beam size increases drastically. This is expected. In the second drift space, the  $y$  beam size increases linearly, while the  $x$  beam size experiences a linear decrease. The second Quadrupole then focuses the  $y$  beam and defocuses the  $x$  beam. This time the defocus of the beam in the  $x$  axis is not as strong as the focusing of the beam in the  $y$  axis. This can be attributed to two factors.

The first is that the strengths of the two magnets are different, hence there is a different level of focus and defocus at each magnet. Secondly, at the second magnet, the beam is much larger than in the  $y$  axis than it was before. Since the focusing force is proportional to the distance from the centre of the magnet, the focusing is much stronger for a larger beam.

At 2.0m from the origin, both dimensions of the beam beam are at their minimum possible size, due to the optimization of the magnets. After that the size rises again because the beam diverges.

Hence, to minimize the beam size at  $z = 2.0$ m, the required  $K$  values of the Magnets should be  $K_1 = 56.942 m^2$  and  $-41.855 m^2$ . Additionally, the first drift distance is also

optimized to be  $d_0 = 0.334$  m

## 4.2 Energy Focusing

This section will focus on finding the maximum beam energy that can be focused by both magnets, as the distance from the origin and between the magnets are varied. It is important to know that  $d_0$  is the first drift space, which is the distance between the plasma source, and the first magnet.  $d_1$  is the distance between the two magnets.

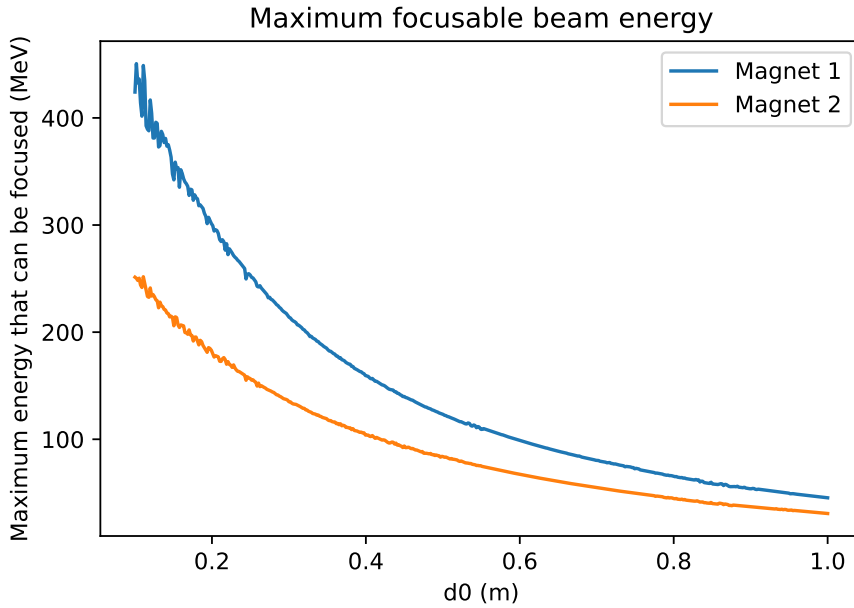


Figure 8: Plot showing the maximum beam energy that can be focused as a function of the distance of the doublet from the origin

We notice in Figure 8 that as  $d_0$  increases, the energy the magnets can focus falls. The significant result here is that magnet 2 consistently remains the magnet that can focus less energy. Hence, magnet 2 is considered the limiting magnet in the beamline. i.e., the maximum overall energy that can be focused will depend on the maximum energy magnet 2 can focus.

Furthermore, the closer the magnets are placed to the exit source, the higher the energies focused are. The reason is that the closer the doublet is to the plasma source, the smaller the electron beam and therefore less transverse momentum being transferred to the electrons at a given transverse offset.

In the same manner, the closer the magnets are to the origin, the smaller the laser diameter they encounter. Since the beam is divergent, the closer the magnet is to

the origin, the smaller its radius of aperture can be. We know from equation 1 that the magnet gradient is inversely related to the square of the radius of aperture of the quadrupoles. Hence, the closer the magnet, the larger its gradient can be. Since the gradient is directly proportional to the energy focused in equation 2, the larger the gradient, the larger the energy focused will be. Therefore, the closer the magnet is to the source, the larger the energy it can focus is.

This is the same reason why magnet 2 will always be the limiting one. Since it will always be further away from the origin than magnet 1, the aperture will have to be bigger, hence it needs to have a smaller gradient, hence can focus smaller energies.

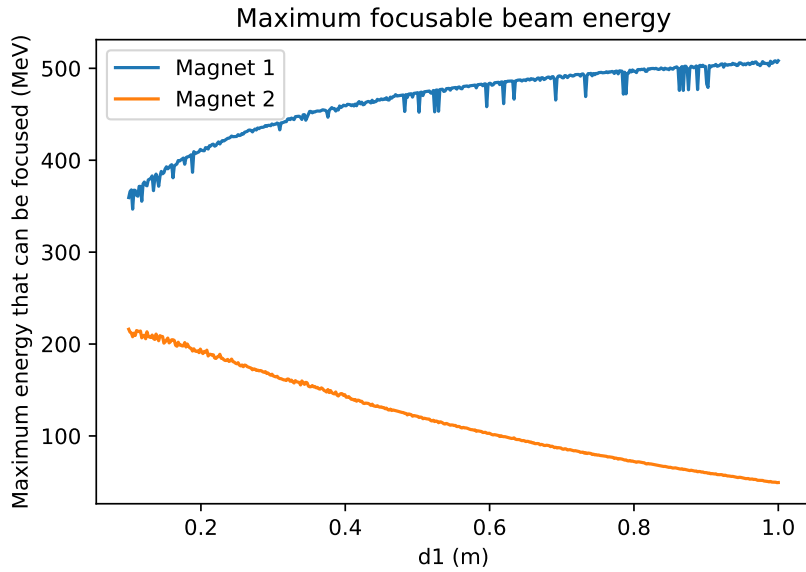


Figure 9: Variation of maximum beam energy that can be focused with distance between magnets.

In the next step, the  $d_0$  is kept constant, and  $d_1$  is varied. Due to the reason given before, Magnet 2 is still the limiting magnet.

This time however the overall energy focused in a plane by Magnet 1 increases with  $d_1$ . The reason being that the further the magnets are from each other, the less magnet 1 has to focus to achieve the same overall focusing.

Therefore, as  $d_1$  increases, the energy focused by magnet 1 also increases, as the focusing done by it gets weaker. However, the energy focused by Magnet 1 has not much practical significance as we are limited by the focusable energy of Magnet 2.

Finally, Figure 10 is a contour plot that gives the maximum focusable energy as a function of both distance from exit source and distance between the magnets.

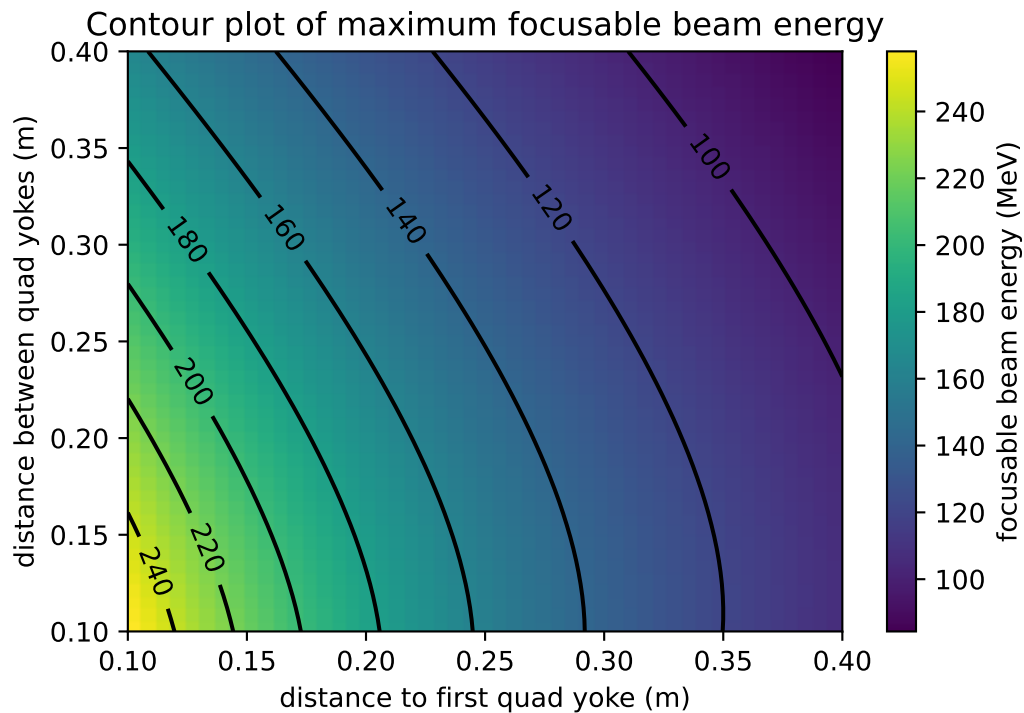


Figure 10: 2D plot of Maximum focusable energy

As the above plots confirm, the best combination where the maximum energy can be focused is when the first magnet is closest to the source, and the space between the magnets is minimum.

Surely, one must also consider practical requirements such as the fact that there must be at least 10cm distance between the magnets, and that the first magnet can not be right at the exit source. Hence, it looks as if the maximum energy that realistically be focused is around 240 MeV.

To confirm the results, the simulation ran a computation of the maximum focusable energy using the values provided in Table 1, and the results were that the maximum focusable energy by Magnet 1 is 386.6 MeV and Magnet 2 is 237.1 MeV. Hence, the results are quite close to those indicated by the contour plot.

## 5 Conclusion

In this report, the basic layout of a compact quadrupole magnet doublet was studied and optimized towards maximum focusable electron beam energy, while ensuring the magnet apertures to allow for a clip-free transmission of the driver laser of a plasma-accelerator.

It was then seen that the maximum beam energy that can be focused depends on factors such as distance from exit source and space between magnets.

As the distance of the magnets from the origin increases, the beam energy they can focus decreases. As the space between the magnets increases, the energy focused by the first magnet increases, while the second one drops. Magnet 2, being the limiting magnet, dictated what the overall maximum focusable energy would be.

Finally, within realistic parameters, the maximum energy that can be focused within the beamline is around 240 MeV, without changing the magnet length or type. Numerically, magnet should be as close to origin as possible which is 10 cm. as close to each other which is 15 cm.

Further studies can be conducted to increase the energy focused by varying the number of magnets, currents, and Magnet yoke lengths. Furthermore, If possible a second doublet could be installed behind the laser out-coupling mirror which could focus the electron beam additionally.

## **6 Acknowledgements**

I would like to begin by thanking the MLS group leader and my supervisor Andreas R.Maier for his support throughout the internship. My appreciation also goes towards Olaf Behnke, Andrea Schrader and the Summer Student programme team for giving us a smooth and amazing experience.

I would also like to thank Prof. Cormac McGuinness and Prof. Mauro Ferreira who made me aware of this internship opportunity and wrote my reference letters.

I would also like to thank my colleagues here Manuel Kirchen, Kaja Schubert and other members of the MLS team for the care they took of me, and allowing me to truly enjoy my work life.

I want to thank the DESY Summer Students of 2022 for one of the most wonderful summers I have had. Every day was an unforgettable experience.

I would like especially express my appreciation for Paul Winkler, who worked closely with me everyday, helping me with questions, doubts, and this report. I am extremely grateful for all the support.

Finally, I would like to thank my parents who encouraged me to apply for this internship, and gave me love and support throughout the application process.

## References

- [1] T. Tajima and J. M. Dawson. Laser electron accelerator. *Phys. Rev. Lett.*, 43:267–270, Jul 1979.
- [2] E. Esarey, C. B. Schroeder, and W. P. Leemans. Physics of laser-driven plasma-based electron accelerators. *Rev. Mod. Phys.*, 81:1229–1285, Aug 2009.
- [3] A. J. Gonsalves, K. Nakamura, J. Daniels, C. Benedetti, C. Pieronek, T. C. H. de Raadt, S. Steinke, J. H. Bin, S. S. Bulanov, J. van Tilborg, C. G. R. Geddes, C. B. Schroeder, Cs. Tóth, E. Esarey, K. Swanson, L. Fan-Chiang, G. Bagdasarov, N. Bobrova, V. Gasilov, G. Korn, P. Sasorov, and W. P. Leemans. Petawatt laser guiding and electron beam acceleration to 8 gev in a laser-heated capillary discharge waveguide. *Phys. Rev. Lett.*, 122:084801, Feb 2019.
- [4] JP Couperus, R Pausch, A Köhler, O Zarini, JM Krämer, M Garten, A Huebl, R Gebhardt, U Helbig, S Bock, K. Zeil, A. Debus, M. Bussmann, U. Schramm, and A. Irman. Demonstration of a beam loaded nanocoulomb-class laser wakefield accelerator. *Nature communications*, 8(1):487, 2017.
- [5] R. Weingartner, S. Raith, A. Popp, S. Chou, J. Wenz, K. Khrennikov, M. Heigoldt, A. R. Maier, N. Kajumba, M. Fuchs, B. Zeitler, F. Krausz, S. Karsch, and F. Grüner. Ultralow emittance electron beams from a laser-wakefield accelerator. *Phys. Rev. ST Accel. Beams*, 15:111302, Nov 2012.
- [6] O. Zarini, A. Köhler, J. Couperus, R. Pausch, T. Kurz, S. Schöbel, H. Meißner, M. Bussmann, U. Schramm, A. Irman, and A. Debus. Advanced methods for temporal reconstruction of modulated electron bunches. In *2018 IEEE Advanced Accelerator Concepts Workshop (AAC)*, pages 1–5, Aug 2018.
- [7] A. R. Maier. 24-hour operation of a laser-plasma accelerator. submitted, 2019.
- [8] Manuel Kirchen, Sören Jalas, Philipp Messner, Paul Winkler, Timo Eichner, Lars Hübner, Thomas Hülsenbusch, Laurids Jeppe, Trupen Parikh, Matthias Schnepf, and Andreas R. Maier. Optimal beam loading in a laser-plasma accelerator. *Phys. Rev. Lett.*, 126:174801, Apr 2021.
- [9] Klaus Floettmann. Some basic features of the beam emittance. *Phys. Rev. ST Accel. Beams*, 6:034202, Mar 2003.
- [10] Stuart Mangles, The John Adams Institute for Accelerator Science Imperial College London . Wakefield acceleration, 2022. [Online; accessed August 21, 2022].
- [11] J. D. Jackson. *Classical Electrodynamics*. John Wiley & Sons, Inc., third edition, 1999.

- [12] CERN. *CAS - CERN Accelerator School : 5th General Accelerator Physics Course: Jyväskylä, Finland 7 - 18 Sep 1992. CAS - CERN Accelerator School : 5th General Accelerator Physics Course*, Geneva, 1994. CERN. 2 volumes, consecutive pagination.
- [13] Helmut Wiedemann. *Particle accelerator physics*. Springer, 2015.
- [14] Helmut Wiedemann. *Single Particle Dynamics*, pages 177–211. Springer International Publishing, Cham, 2015.
- [15] Helmut Wiedemann. *Particle Beams and Phase Space*, pages 213–251. Springer International Publishing, Cham, 2015.